

DRAFT GT2006-91157

## FLAME PROPAGATION FOLLOWING THE AUTOIGNITION OF AXISYMMETRIC HYDROGEN, ACETYLENE AND NORMAL-HEPTANE PLUMES IN TURBULENT CO-FLOWS OF HOT AIR

Christos N. Markides, and Epaminondas Mastorakos

Hopkinson Laboratory, Department of Engineering, University of Cambridge, Trumpington Street, CB2 1PZ, U.K.

### ABSTRACT

Axisymmetric plumes of hydrogen, acetylene or n-heptane were formed by the continuous injection of (pure or nitrogen-diluted) fuel into turbulent co-flows of hot air. Autoignition and subsequent flame propagation was visualized with a high-speed intensified camera. The resulting phenomena include the 'Flashback' and statistically steady 'Random Spots' regimes. It was found that with higher velocities and smaller injector diameters, the boundary between Flashback and Random Spots shifted to higher air temperatures. In the Random Spots regime, the autoignition regions moved closer to the injector with increasing air temperature and/or decreasing air velocity. After a localized explosive autoignition event, flames propagated into the unburnt mixture in all directions and eventually extinguished, giving rise to autoignition 'spots' of mean radius 2–5mm for hydrogen and 6–10mm for the hydrocarbons. The average flame propagation velocity in both the axial and radial directions varied between 0.5 and 1.2 times the laminar burning speed of the stoichiometric mixture, increasing as the autoigniting regions shifted upstream.

Keywords: Kernel Growth, Flame Propagation, Flame Velocity, Autoignition, Flashback.

### INTRODUCTION

Recently, the inhomogeneous (non-premixed) autoignition of axisymmetric nitrogen-diluted hydrogen [1, 2], acetylene [2] and normal (n)-heptane [2, 3] plumes in turbulent co-flows of pre-heated air has been studied experimentally. Measurements and observations have shown that the emergence of autoignition leads inevitably towards either a full flame establishment or a short-lived flame. The autoignition and post-ignition combustion phenomena consisted of the following three stages, as illustrated in Fig. 1 with a trace of global emission from hydroxyl radical chemiluminescence (OH\*) taken with a Photo-Multiplier Tube (PMT) and simultaneous direct high-speed OH\* images. Initially, an explosive autoignition event (or autoignition kernel) appeared at a well-defined, but random location and instant.

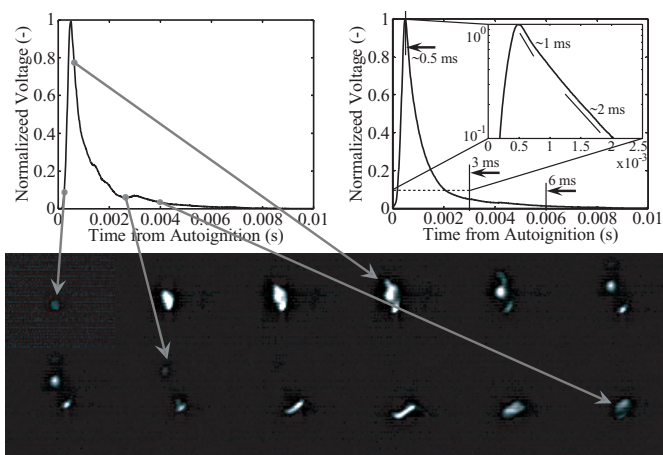


**Figure 1. Top-left: Typical instantaneous PMT (with OH\* filter) voltage profile of single acetylene autoignition 'spot'. Top-right: Average PMT OH\* profile (over many such as that shown on left). Bottom: Fast OH\* image sequence (left-to-right and top-to-bottom) taken simultaneously with the PMT measurement shown on top-left at 10kHz. Flow direction upwards. Reproduced from [2].**

Following this, unsteady flamelets propagated into the surrounding unburnt, high-temperature inhomogeneous mixture, whose composition can be characterized by the mixture fraction ( $\xi$ ) or equivalence ratio ( $\phi$ ). The post-ignition flames either gradually extinguished in relative proximity to the original point of autoignition ('Random Spots' regime), or propagated upstream to give rise to a normal, fully-fledged non-premixed flame stabilized on the injector rim if the injection velocities were low enough ('Flashback' regime), or a lifted flame if the velocities were high enough ('Lifted Flame' regime) [1, 2]. It is interesting to explore further these phenomena; particularly the flame propagation phase following localized autoignition since this constitutes a dangerous situation in the premix ducts of lean-premixed gas turbines and may be relevant in Homogeneous Charge Compression Ignition (HCCI) and diesel engines. The authors are not aware of

previous investigations concerned with the fate of these post-ignition flames in such a configuration, nor with the conditions that mark the delineation towards the possibility of flashback.

Flame propagation in homogeneous mixtures has been extensively investigated in both continuous flow configurations [4] and combustion vessels [5]. In the case of successful forced (spark) ignition of inhomogeneous mixtures, the flame front propagates upstream along the stoichiometric mixture fraction ( $\xi_{ST}$ ) iso-surface, as a triple or edge flame depending on the local strain rate, with a speed 2-5 times the laminar burning velocity of a stoichiometric mixture ( $S_L$ ) [6, 7]. In the case of flame initiation due to autoignition, as in the experiments described here, the initial, explosive appearance of the flame, although randomly located in space, occurs at a well-defined (and *a priori* easily estimated) instantaneous  $\xi$  termed the ‘most reactive’ mixture fraction ( $\xi_{MR}$ ) [8]. As the flame travels, it progresses through regions of inhomogeneous mixture that is chemically ‘close to autoignition’, meaning that it has been reacting in the hot environment and has an evolved radical pool relative to cold/frozen conditions. This may be expected to have an impact in the overall flame speed and so the edge flame speed in inhomogeneous mixtures following autoignition, as in diesel engines, may be expected to be different from the edge flame speed in spark-ignition situations, as in the ignition of non-premixed flames in various combustors.

The autoignition of transient diesel sprays in engine combustion chambers has been visualized with high-speed photography [9, 10], as has HCCI combustion [11]. In contrast, images of autoignition and subsequent post-ignition flame propagation of gaseous fuel plumes in any continuous flow apparatus are almost non-existent. Direct Numerical Simulations (DNS) of flame propagation following autoignition in turbulent mixing layers have shown that, following localized autoignition at  $\xi_{MR}$ , the flame propagates across the layer with a velocity of the order of (or even slightly less than)  $S_L$  [8]. Given the fact that in the simulations the mixture surrounding the autoignition kernel is itself chemically evolved, this speed is considered relatively low. More measurements are necessary to improve our understanding of the flame propagation processes in this ‘premixed phase’ of diesel engine combustion.

This work aims to describe the observed operating regimes, to quantify the conditions demarking the onset of ‘Flashback’, to provide high spatial and temporal resolution images of the flame fronts and to supply data on the velocity of the flame originating from the autoignition spots. To this end, we have measured the propagation velocities of flamelets following localized autoignition in the case of nitrogen-diluted hydrogen, acetylene and n-heptane plumes injected concentrically into turbulent co-flows of hot air, with high-speed OH\* imaging.

## EXPERIMENTAL METHODS

### Apparatus

Figure 2 shows the apparatus, which has previously been used to study mixing [12] and autoignition [1-3] in axisymmetric co-flows. A detailed description can be found in Markides [2], but below we provide a summary of the most relevant points to the aims of this paper.

<sup>1</sup> Quantities are reported to the least significant figure allowed by the uncertainty. Uncertainties are relative and are reported at one significant figure and 95% confidence level (or a confidence interval of two standard deviations).

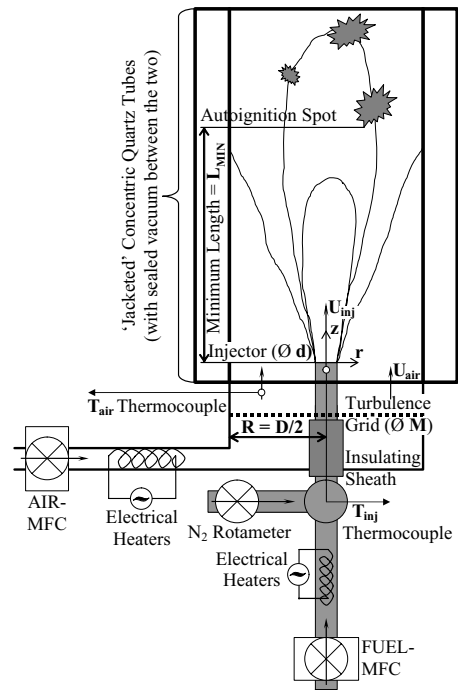


Figure 2. Apparatus sketch.

Compressed laboratory air at a regulated backpressure of  $10.0 \pm 0.5 \text{ bar}^1$  was filtered, dried and fed to a Bronkhorst High-Tech digital, thermal mass flow controller (AIR-MFC). The AIR-MFC had the following technical specifications: an accuracy of  $\pm 0.5\%$  of reading plus  $\pm 0.1\%$  of full-scale and a reproducibility of  $0.1\%$  of full-scale. The indeterminate (random) uncertainty in the measurement of the air mass flow ( $\dot{m}_{air}$ ) is not more than  $\pm 1\%$ . Further downstream the air was heated by four low-cost high-temperature inline electrical resistance heaters that were developed in-house. Measurements of the air temperature at the exit of the heaters were employed as negative feedback inputs into Proportional-Integral-Derivative (PID) temperature controllers that were manually pre-tuned and used to control the voltage supplies to the heaters to minimize temperature gradients and drifts. During the measurements, with a constant pre-set reference temperature and steady flow of air, the instantaneous deviation of the measured air temperature from the reference never exceeded  $1^\circ\text{C}$  (obtained with a  $0.20\text{mm}$  diameter, R-Type thermocouple wire with a response time constant of  $\approx 0.3\text{s}$ ). After the heaters, a perforated plate of 44% solidity and with circular,  $3.0\text{mm}$  diameter ( $M$ ) holes was used for turbulence generation, followed by a final section consisting of a  $35.0\text{mm}$  contraction length, designed to inhibit boundary layer growth, promote uniform velocity and temperature conditions and minimize flow separation and unsteadiness leading in to the test section. The main experiment flow section consisted of a vertically orientated  $0.50\text{m}$ -long cylindrical quartz tube, of inner diameter ( $D$ )  $25.00 \pm 0.03\text{mm}$  (and inner radius  $R$ ), open to atmosphere. The ‘jacketed’ (two sealed concentric) quartz tube configuration incorporated a pre-evacuated annular volume to reduce heat losses and maintain uniform temperature conditions in the flow, while providing full optical access and requiring no additional insulation. The complete assembly (excluding the quartz tube) was heavily insulated with a  $150\text{mm}$  thick lagging layer of non-refractory ceramic blankets along its whole length.

At the inlet of the quartz tube, which was 26mm upstream of the injector nozzle exit, a twin-bore ceramic-sheathed, 0.2mm diameter, bare-wire, butt-welded R-Type thermocouple was embedded in the wall and protruded by  $9\pm 1$ mm into the flow, with horizontal orientation. This was used to measure the bulk air temperature at the inlet ( $T_{air}$ ). The raw  $T_{air}$  reading was corrected for both radiative and conductive heat losses. Typically, the heat loss correction can be broken down into: radiative heat losses of 0.2% at low temperatures ( $\approx 800$ K), increasing to 0.4–0.5% at high temperatures ( $\approx 1100$ K), and, conductive losses of 0.2% at low flow velocities ( $< 20$ m/s), increasing to 0.4–0.5% at high flow velocities ( $> 20$ m/s). After correction, the reported  $T_{air}$  is associated with an indeterminate uncertainty of  $\pm 0.3\%$  and a determinate uncertainty of  $\pm 0.6\%$ . Air with  $T_{air}$  up to 1200K has been utilized for the experiments mentioned in this paper.

Two gaseous fuels were used: hydrogen (99.999% vol/vol purity) and acetylene (99.6% vol/vol purity), supplied from compressed cylinders. Their mass flow rates were set and measured with a Bronkhorst High-Tech digital, thermal mass flow controller (FUEL-MFC). The measurement of the fuel mass flow rate ( $m_{fuel}$ ) had a 1% determinate (systematic) and  $\pm 0.8$ –3% indeterminate uncertainty, the latter decreasing at higher  $m_{fuel}$ . In addition to these fuels, n-heptane was also used, which is a liquid at room temperature and pressure and was thus pre-vaporized. A pre-calibrated positive displacement peristaltic pump and small electric heater were used for this purpose. The capability of the pump to set the mass flow of n-heptane is associated with a worst-case error of  $\pm 6\%$  for the lowest flow rates, improving to  $\pm 4\%$  for the highest.

Nitrogen was supplied from a compressed cylinder (99.9995% vol/vol purity). Flow rate adjustment and measurement was achieved with a pair of suitably ranged coarse/fine pre-calibrated rotameters, equipped with pressure gauges at their exits. The pressure and ambient temperature variations were taken into account (by means of their effect on the density) for corrections to the raw indicated flow rates. The total indeterminate uncertainty in the measurement of the mass flow rate of nitrogen ( $m_{N_2}$ ) is  $\pm 6$ –10%. For the n-heptane experiments, the FUEL-MFC was used instead of the rotameters, improving the nitrogen mass flow indeterminate uncertainty to  $\pm 3$ –6%. Intense mixing promoted the thorough dilution of the pure fuel with nitrogen, resulting in diluted-nitrogen fuel mixtures that will be referred to as ‘diluted-fuel’ or ‘injected stream’. The total ‘injected stream’ mass flow rate ( $m_{inj}$ ) was equal to the pure fuel plus nitrogen mass flow rates,  $m_{inj} = m_{fuel} + m_{N_2}$ . In addition, the injected stream dilution will be described by the mass fraction of fuel in the diluted-fuel mixture ( $Y_{fuel}$ ). The total uncertainty in  $Y_{fuel}$  is up to  $\pm 5$ –7% for hydrogen and acetylene, improving to  $\pm 3\%$  for n-heptane.

The pure or nitrogen-diluted fuel was injected into the quartz tube axially and continuously through a  $2.24\pm 0.03$ mm inner ( $d$ ) and  $2.96\pm 0.02$ mm outer ( $d_o$ ) diameter, stainless steel thin-walled hypodermic tube injector at ambient pressure. The injector was positioned at the centerline of the quartz tube, with the nozzle exit 63mm downstream of the perforated plate in order to allow the turbulence to develop. For most of its length, the injector tube was encased in a 2.0mm thick-walled ceramic sheath to insulate the fuel from the hot air, keep it at a cooler temperature and inhibit fuel decomposition prior to injection. A 500mm long and 0.25mm diameter, stainless steel sheathed,

mineral insulated K-Type thermocouple was placed through the injector all the way to the injection location and allowed for a real time measurement of the fuel stream injection temperature ( $T_{inj}$ ). It is noted that, in general,  $T_{inj}$  in these experiments depended on forced convective heat transfer from the hot co-flow air, through the stainless steel injector tube walls, to the fuel flowing inside the injector and ranged from about 600 to 1100K, with a  $\pm 0.8\%$  uncertainty.

### **Flow Condition Characterization**

Let  $r$  denote the radial distance from the centerline of the tube and  $z$  the axial distance from the injector. The inlet bulk air velocity ( $U_{air}$ ) is defined as the cross-sectional volumetric averaged velocity based on  $m_{air}$ , the density of air at inlet conditions ( $T_{air}$  and ambient pressure) and the annular area defined by the outer injector wall and the inner quartz tube extent ( $d_o/2 < r < R$ ), i.e.  $\pi/4(D^2 - d_o^2)$ . To describe the dynamic condition of the air stream at the inlet of the quartz tube, we define a turbulent Reynolds number,  $Re_{turb} = u'_{air} L_{turb} / \nu_{air}$ . Here,  $u'_{air}$  is the root mean square (rms) of the turbulent fluctuations of the axial velocity,  $L_{turb}$  the integral turbulent lengthscale and  $\nu_{air}$  the kinematic viscosity of air, all at the quartz tube inlet. In the experiments presented this paper,  $U_{air}$  ranged between 10 and 35m/s (with a total uncertainty of 1.5%) and  $Re_{turb}$  between 40 and 200. The injected diluted-fuel stream velocity ( $U_{inj}$ ) is based on  $m_{inj}$ , the flow area of the injector  $\pi d^2/4$ , and, the diluted-fuel stream density at  $T_{inj}$  and ambient pressure. The uncertainty in the measurement (and consequently setting) of  $U_{inj}$  was within  $\pm 4\%$  for acetylene and  $\pm 6\%$  for n-heptane. In this paper, we concentrate on experiments in which  $U_{inj}$  was adjusted to attain ‘equal velocity’ flow and mixing conditions. For this requirement, the normalized injection velocity ( $v_{inj}$ ), defined as  $v_{inj} = U_{inj} / U_{air}$ , was set to be nearly equal to unity, with worst-case deviations of 20%, or  $v_{inj} = 1.00\pm 0.20$ . It is important to note that the injected flow is not a jet, but rather a low momentum release into the co-flow. Consequently, the flow field, as well as the resulting plumes, will be momentum-dominated by the background turbulence in the co-flow [12].

In this paper, we correlate measurements of the flame propagation phenomena with the reported inlet conditions. This is done based on the understanding that the complete flow field (velocities, temperatures and scalar mixing) conditions inside the tube during autoignition/combustion, can be fully and uniquely described by the aforementioned reported inlet measurements ( $T_{air}$ ,  $T_{inj}$ ,  $U_{air}$ ,  $v_{inj}$  and  $Y_{fuel}$ ). To assist future modeling attempts of these phenomena and to inspect the full conditions inside the tube and their relation to the reported inlet variables, we performed cold and hot flow characterization experiments, described collectively by the lack of autoignition/combustion in the tube.

A Dantec constant temperature anemometer system with a 1.25mm long, 5 $\mu$ m diameter hot wire was used to measure axial velocities, with and without injected flow, at cold (room) conditions. Aiming to replicate the autoignition conditions as closely as possible, the cold flows were set to exhibit Reynolds number similarity with the hot (autoignition) flows. The injection velocity was then set to achieve ‘equal velocity’. Measurements of the local mean axial velocity  $U$  showed that the ratio  $U/U_{air}$  was about 1.15 in the region away from the injector and quartz tube wall boundary layers ( $0.08 < r/D < 0.42$ ,  $z=0$ ). From the root mean square (rms) of the fluctuation of the

local axial velocity ( $u'$ ),  $u = \langle u'^2 \rangle^{1/2}$ , the normalized rms intensity  $u/U$  at ( $r/D \approx 0.25$ ,  $z=0$ ) was 0.14–0.15, decaying to 0.10 by 42mm downstream. The integral lengthscale  $L_{\text{turb}}$  was obtained by integrating over the normalized autocorrelation function of  $u'$  and the use of Taylor's hypothesis. At ( $r/D \approx 0.25$ ,  $z=0$ ) it was found to be 3–4mm, i.e. of the order of the grid hole size, increasing by 1mm in the first 42mm downstream. Power spectra and probability density functions showed that the co-flow was turbulent and near-homogeneous, as expected. Radial profiles of  $U$  were also taken at representative autoignition temperatures with a high-temperature Pitot tube and thermocouple used in close proximity, the latter to measure the local temperature and hence evaluate the local air density. At these elevated temperatures the presence of the temperature boundary layer and the finite heat losses to the wall caused the velocity boundary layer to thicken, reducing the region of uniformity to  $r/R = 0.10$ – $0.65$ . Finally, a high-temperature hot wire was employed at a single hot condition ( $T_{\text{air}} = 800\text{K}$  and  $U_{\text{air}} = 20.6\text{m/s}$ ) and single location in the flow ( $r/R=0.5$ ,  $z=0$ ) to obtain  $u/U$  that was found to be between 0.05–0.10.

The local absolute temperature  $T$  was measured with a fine 76 $\mu\text{m}$  diameter, K-Type thermocouple wire ( $\approx 0.04\text{s}$  time constant). In addition, the fluctuations  $T'$  were obtained after compensation for the finite time constant of the wire in the frequency domain [2]. The thermocouple measurements have shown that the (local) mean temperature into the tube  $\langle T \rangle$  was uniform for  $r/R = 0.15$ – $0.60$ , down to  $z = 80\text{mm}$ . Axially,  $\langle T \rangle$  dropped linearly by 10K in the first 100mm due to heat losses. The rms of the temperature fluctuations,  $\langle T'^2 \rangle^{1/2}$ , were found to be small relative to  $\langle T \rangle$ , with values of  $\langle T'^2 \rangle^{1/2} / \langle T \rangle$  in the range 0.05–0.25%, affirmed both by a high-temperature hot wire and a compensated fine thermocouple. This corresponds to about 0.5–2.5K. Finally, the normalized cross-correlations of velocity and temperature fluctuations,  $\langle u'T' \rangle / U \langle T \rangle$ , were small with an indicative value of  $5 \times 10^{-6}$ . The temperature fluctuations were well described by a normal (Gaussian) process.

To simulate and understand the axisymmetric mixing field formed by the continuous, concentric injection of fuel from the finite-sized nozzle into the confined turbulent air co-flows, high-resolution two-dimensional acetone Planar Laser-Induced Fluorescence (PLIF) measurements of the conserved scalar  $\xi$  were performed at low temperatures ( $T_{\text{air}} = 473\text{K}$ ). For an extensive description of these experiments and data on the mixing field in this configuration, see Markides and Mastorakos [12]. Briefly, measurements of the local concentration of the injected fuel were suitably normalized to obtain the  $\xi$  field from relatively close lengths to the source to a downstream distance of about 60–70mm, or 30d. The two-dimensional scalar dissipation rate  $\chi_{2D}$  was calculated from the sum of the axial and radial gradients of the measured planar  $\xi$ . Measurements of the mean  $\xi$  were consistent with the Gaussian plume equation, with the resulting plumes having Gaussian radial profiles and axial decay in the far field as expected from previous studies. The plumes were initially relatively thin and short, with the  $\langle \xi \rangle = 0.1$  iso-contour occupying radial lengths of  $r/d < 1.5$ , or  $r/R < 0.15$  and axial lengths along the centerline up to 8d, or 20mm. The variance  $\langle \xi'^2 \rangle$ , increased to a maximum and then decayed downstream. The rms  $\xi'$  normalized by the mean, increased from zero close to the source, to a value of about 4 downstream for these equal velocity flows. The above allow one to reason that, initially, the mixing will occur in

regions of relatively uniform velocity, but also, that downstream the plume will quickly diffuse into the tube. The full, mean three-dimensional  $\chi_{3D}$  was estimated by symmetry, in the mean, along the centerline. This was adequately described by the timescale ratio model, with  $C_D=2$  for axial distances corresponding to a residence time greater than 0.1–0.2  $k/\epsilon$  turbulent timescales and radial distances  $r/d < 1$ , where  $k$  is the turbulence kinetic energy and  $\epsilon$  its mean dissipation.

### **Autoignition Achievement**

Approximately 1–2 hours were required for the heat-up process, during which the apparatus temperature was gradually increased until it reached the desired temperature necessary for autoignition. Steady operation was allowed for about 1 hour at the elevated temperature for the apparatus to reach thermal equilibrium. At this stage, fuel flow would be allowed. The fuel and nitrogen flow rates were adjusted to get the desired diluted-fuel composition. With continuous injection of the correct diluted-fuel, autoignition would be detected in the tube. However, autoignition was allowed to continue for 1–2 minutes before any measurement was taken, to permit final adjustments and to ensure that transients had decayed and drifts had been minimized. At this point, the raw  $T_{\text{air}}$ ,  $T_{\text{inj}}$  and the flow rates of the air, fuel and nitrogen were recorded.

As previously mentioned, it was found that depending on the conditions, various regimes of operation were possible, including such behavior as ‘Random Spots’ and ‘Flashback’, with the latter being dominant at higher  $T_{\text{air}}$  and lower  $U_{\text{air}}$ . The transient, short-lived autoignition-propagation-extinction of a ‘spot’, such as the one in Fig. 1, whereby each autoignition event was associated with flamelets that extinguished in relative proximity to the original autoignition site, was only possible in the Random Spots regime. In contrast, in the Flashback regime the flame did not extinguish and propagated upstream with increasing size and intensity. The first appearance of autoignition was quickly followed by the establishment of a fully-fledged, large-scale diffusion flame on the injector. Figure 3 shows a typical Flashback sequence.

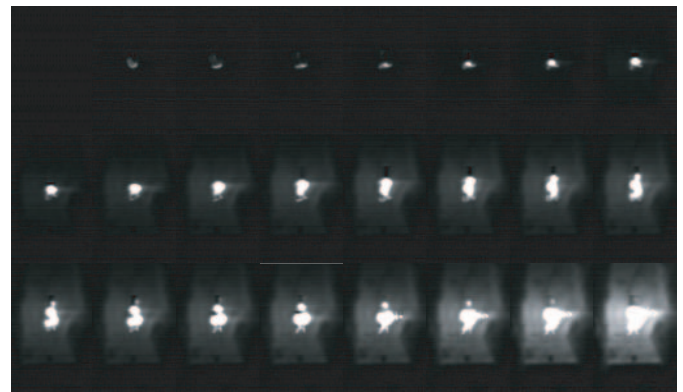


**Figure 3. Acetylene autoignition and flashback. Fast image sequence (left-to-right, top-to-bottom) at 13.5kHz. Conditions  $T_{\text{air}} = 809\text{K}$ ,  $U_{\text{air}} = 10.4\text{m/s}$ ,  $u_{\text{inj}} = 0.93$ ,  $Y_{\text{C}_2\text{H}_2} = 0.75$ . Flow direction upwards.**

It is interesting to examine the exact conditions for which such behavior is possible. The hydrogen Flashback transition is presented in Fig. 4. In Fig. 4(a), the data points and lines mark the boundaries of the lowest  $T_{\text{air}}$  necessary at a particular  $U_{\text{air}}$  to

cause the first instance of Flashback (lower bound). Data is shown for four different values of  $v_{inj}$  as indicated in the legend. For a given dilution then, in this case  $Y_{H_2} = 0.15$ , the  $T_{air}$  necessary for Flashback increases with increasing  $U_{air}$  and  $v_{inj}$ . In Fig. 4(b) below, all the data points indicate the possibility of Random Spots behavior. For a given  $U_{air}$ , increasing  $T_{air}$  beyond the limit noted by the solid (for  $Y_{H_2} = 1$ ) or dashed (for  $Y_{H_2} = 0.05-0.40$ ) resulted in Flashback. With all else being fixed, the effect of increased dilution is to increase considerably the  $T_{air}$  necessary for Flashback. Finally, experiments with the smaller injector<sup>2</sup>,  $d = 1.03\text{mm}$ , (not shown) revealed that the possibility of Flashback was greatly reduced.

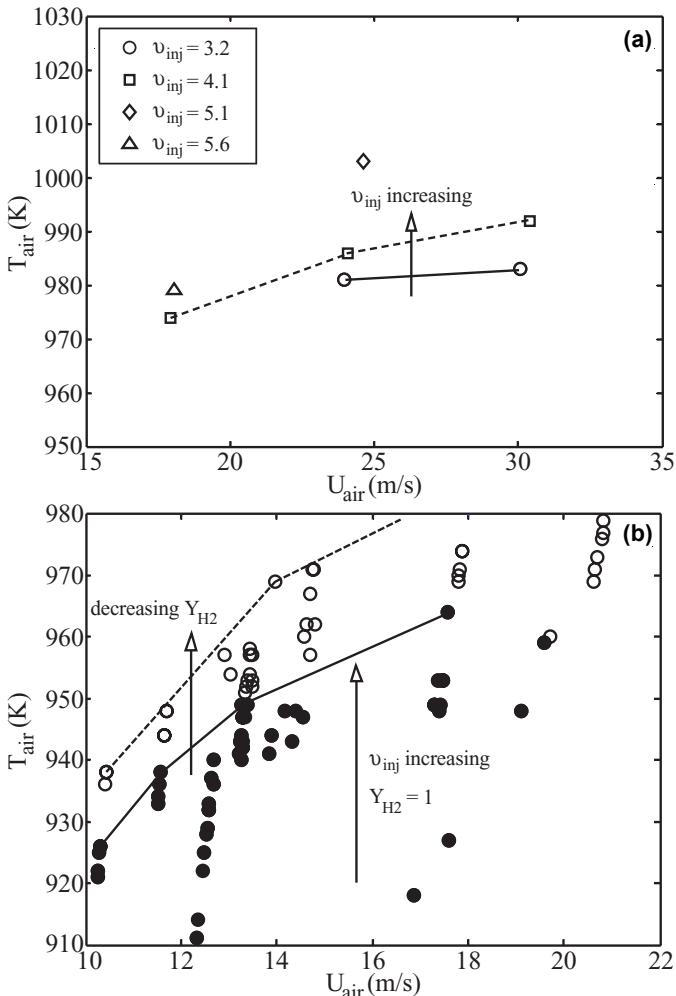


**Figure 4. Temperature—Velocity operation envelope limits for hydrogen. (a)  $Y_{H_2}$  fixed to 0.15. Data points signify transition limit to 'Flashback'. (b) Filled data points are for  $Y_{H_2} = 1.00$ ,  $u_{inj} = 3.2-5.6$ . Empty data points for  $Y_{H_2} = 0.05-0.40$ ,  $u_{inj} = 0.35-12.6$ . Data points signify stable 'Random Spots' behavior; lines signify transition limit to 'Flashback'.**

Therefore, in summary, the onset of Flashback shifted to higher  $T_{air}$  with: higher  $U_{air}$ , higher  $v_{inj}$  and smaller  $d$ . We now turn our attention to the velocity of propagation of the autoignition 'spots' in the Random Spots regime. Here, autoignition occurs repeatedly and flamelets exist and

<sup>2</sup> Recall (bottom left, page 3) that the default injector had  $d = 2.24\text{mm}$ .

propagate, but on a local scale only and in close proximity to the original autoignition sites. The short-lived nature of each flamelet due to extinction minimizes the contamination of its observations by other post-ignition flames.

### Measurement, Processing, Analysis and Calculations

A custom intensified Complementary Metal Oxide Semiconductor (CMOS) system, capable of high-speed, UV-sensitive imaging was used to provide fast  $OH^*$  chemiluminescence image sequences showing both the process of the explosive emergence of autoignition and of the subsequent unsteady, post-ignition flamelet propagation. It consisted of a 10-bit Phantom v.4.2 CMOS camera and a C9546-04MP46 Hamamatsu intensifier. As with most CMOS cameras, the image size is linked to the potential framing rate. Typically, in this work,  $500 \times 100$  pixel imaging areas were utilized allowing frame rates of up to 12kHz. The intensified CMOS was used with a UV-lens and a further  $OH^*$  optical filter, band-centered at  $307 \pm 1\text{nm}$ . The Nikkor lens has a nominal focal length of 105mm and a maximum aperture of  $f/4.5$ . It was operated fully open to capture the weak chemiluminescence signals.

Each of the near-instantaneous fast images was examined for the axial and radial location and extent of the autoignition 'spots' and the 'thickness' of the flame fronts. These direct measurements were used to calculate the absolute post-ignition velocities of: (i) the longitudinal advection of the 'spots', (ii) the longitudinal propagation of the upstream flame fronts, and, (iii) the transverse propagation of the radial (left and right) flame fronts, originating at the autoignition sites, as described in this section (below). In turn, the absolute velocities were used to estimate the velocities with which the flames propagated upstream relative to the oncoming unburnt flow, which were then compared with the laminar premixed flame speeds at representative conditions and mixture compositions.

At this stage, it is useful to define the length and velocity variables used in this paper. Figure 5 shows an instantaneous autoignition 'spot' and demonstrates the various lengths, based on displacement distances relative to the injector and centerline.

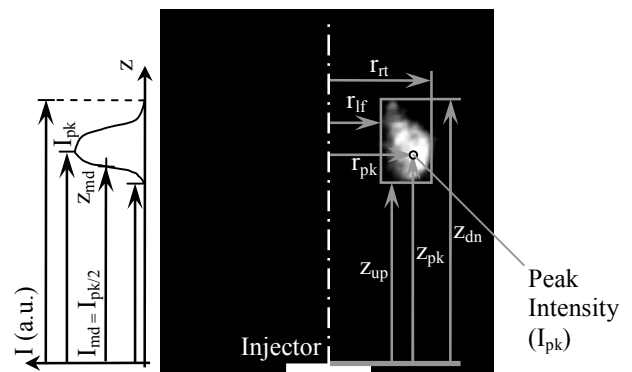


**Figure 5. 'Autoignition spot' definitions. Flow upwards. Vectors showing positive direction.**

The longitudinal half-size of the spot can be obtained from the difference between the downstream and upstream extents of the spot,  $Z_{spot} = (z_{dn} - z_{up})/2$ . Similarly, the transverse half-size of the spot is,  $R_{spot} = (r_{out} - r_{in})/2$ . The geometric centerline of the spot ( $s_{rad} = r_{in} + R_{spot}$ ,  $s_{ax} = z_{up} + Z_{spot}$ ) does not necessarily coincide with the point of peak intensity ( $I_{pk}$ ), which we denote by  $(r_{pk}, z_{pk})$ .

Nevertheless, we do not expect these two points to be far from each other and in fact, measurements have shown that in the mean, the point of peak intensity was closer to the injector than the geometric center by less than  $0.05\langle Z_{\text{spot}} \rangle$ . Additionally, we define a measure of the ‘steepness’ of the spot upstream flame ‘thickness’,  $\Delta = z_{\text{md}} - z_{\text{up}}$ , as the distance between  $z_{\text{up}}$  and the minimum axial length  $z_{\text{md}}$  from the injector at which the intensity of the spot reaches half the peak value,  $I_{\text{md}} = I_{\text{pk}}/2$ . Absolute longitudinal velocities are defined based on these displacements. The absolute upstream flame front velocity is  $U_{\text{up}} = dz_{\text{up}}/dt$ , while the longitudinal advection velocity of the spot can be either  $U_{\text{spot}} = ds_{\text{ax}}/dt$ , or  $U_{\text{spot}} = dz_{\text{pk}}/dt$ , since  $s_{\text{ax}}$  and  $z_{\text{pk}}$  are similar. Here, we choose the latter for reasons that are explained in the ‘Flame Front and A/Ignition Spot Advection Velocities’ section. Relative longitudinal velocities that are used include the velocity of the upstream flame front relative to the oncoming flow,  $S_T = U_{\text{up}} - U_{\text{air}}$ . Finally, the (absolute and relative) transverse flame velocity is,  $V_{\text{spot}} = dR_{\text{spot}}/dt$ .

From separate PMT measurements, but also directly from the fast image sequences, we know that the standard deviation (std) of the upstream flame front propagation velocity, normalized by its mean, lies between 0.2 and 0.6, with 0.4 a more representative median value. Hence, in order to provide a converged measurement of the mean velocity during a single run of given conditions, to within (say) 10% statistical uncertainty and 95% confidence interval, it would be necessary to make measurements from about 70 flames. Furthermore, from the same measurements it was found that the propagation velocities were a function of the time from explosive autoignition (see Fig. 1, but also Fig. 13). In order to overcome this problem and report on a single value of velocity for each flame, we define any propagation velocity as the average distance traveled from the moment of explosive autoignition, i.e. corresponding to the maximum in Fig. 1, to the time the chemiluminescence intensity reaches 5% of its maximum value. Then, to achieve a respectable temporal resolution we required (on average) at least 20 images per flame. This, together with the condition for converged statistics, translate into a requirement for the evaluation of at least 1400 instantaneous images for a single flame velocity measurement. Clearly, it is difficult to achieve this goal with a manual investigation of the fast image sequences. Here, these actions were performed by an automated process.

A flame tracking script was used to examine the axial and radial flame fronts, as defined in Fig. 5. In the measurements presented here, 10,000 images were recorded on average per run (set of conditions). Collectively, for the three fuels tested in this way, about 50 conditions were tested, resulting in 1/2 million images that had to be processed for the four distinct longitudinal and three transverse definitions of the flame location. The indeterminate uncertainty in locating the flame front in any image is 5%, corresponding to a velocity of 0.6m/s. The worst-case determinate uncertainty arising from the arbitrary thresholding applied to differentiate between different ‘spots’ in the same image and hence the correct tracking of the same ‘spot’ throughout its ‘lifetime’ is 2%.

Finally, the measured relative longitudinal and transverse velocities were compared with  $S_L$ . The laminar flame speeds of hydrogen, acetylene and n-heptane were obtained with RUN1DL [13], a premixed laminar flame solver with detailed

molecular transport and reaction kinetics [14-16], at the supplied conditions and nitrogen-dilution, but for stoichiometric air–fuel balance. The premixed flame equations in RUN1DL return  $S_L$  as a solution to a problem that has boundary condition of zero reaction rate at the unreacted/cold boundary. Inescapably, this is not strictly so due to autoignition at the high temperatures employed and hence  $S_L$  is a function of location of the flame from the cold boundary. This uncertainty of the predicted  $S_L$  was estimated at  $\pm 3-5\%$  by a sensitivity analysis to the location of the flame from the boundary.

All data are presented as a function of the minimum autoignition length  $L_{\text{MIN}}$ . As demonstrated in Fig. 2,  $L_{\text{MIN}}$  is defined as the minimum axial distance from the injector at which autoignition was observed during a run and can be related to other measures of autoignition length [1-3].

## RESULTS AND DISCUSSION

### Flame Front Thickness and A/Ignition Spot Size

To assess the quality of the measurements, we first probe the results for the lengths in Fig. 5, from which the velocities were calculated. Probability density functions (pdfs) of the longitudinal upstream flame front thickness  $\Delta$  (solid) and spot half-size  $Z_{\text{spot}}$  (dash-dot), for n-heptane are shown in Fig. 6.

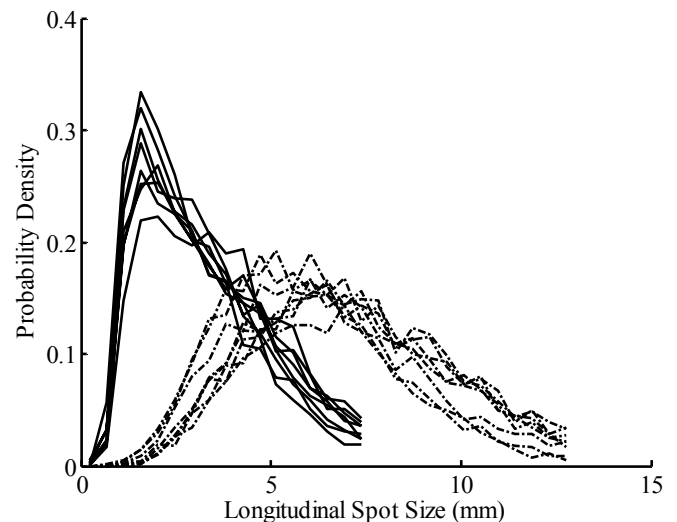


**Figure 6. Pdfs of upstream flame front thickness (solid) and autoignition spot half-size (dash-dot) for n-heptane with:  $T_{\text{air}} = 1100-1140\text{K}$ ,  $U_{\text{air}} = 14$  and  $18\text{m/s}$ ,  $Y_{\text{fuel}} = 0.95$ , and,  $u_{\text{inj}} = 1.0-1.2$ .**

All pdfs are negatively skewed, biased towards the injector, but especially the thickness pdfs. This agrees with the independent finding that the spots occur in bursts [2], such that isolated, independent events of a nominal size are succeeded intermittently by a sequence of spots that propagate and give rise to secondary spots away from the initial point of (primary) explosion. Generally, it is difficult to distinguish (even by eye) between primary and secondary events and so the effective thickness and spot size increase. The probability of  $Z_{\text{spot}}$  being larger than  $D/2$  ( $= R = 12.5\text{mm}$ ) is about 3–15% of its maximum. Given the (on average) ellipsoid ( $\langle Z_{\text{spot}} \rangle / \langle R_{\text{spot}} \rangle = 1.1 \pm 0.1$ ) appearance of the spots, this suggests that the spot flame fronts are correctly captured to within 10% by the flame

tracking script, as we anticipate the spot to quench at the tube inner wall, thus limiting its maximum radial size to  $R_{\text{spot}} < D/2$ . Consider now the mean longitudinal autoignition spot half-size  $\langle Z_{\text{spot}} \rangle$  (empty symbols) and upstream flame front thickness  $\langle \Delta \rangle$  (filled symbols) for n-heptane as shown in Fig. 7.

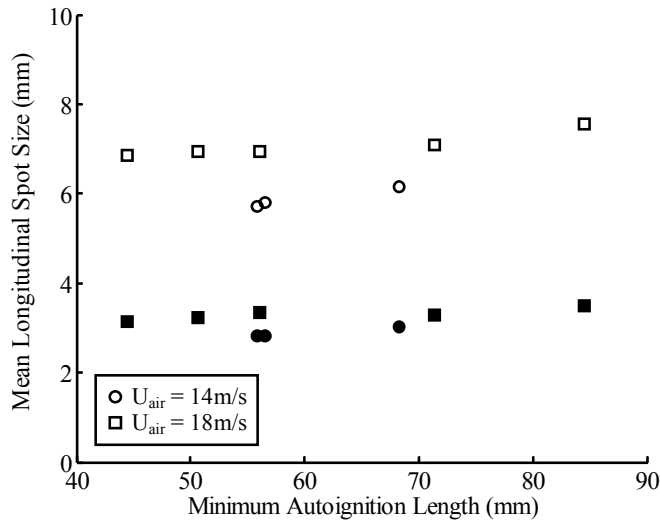


**Figure 7. Mean upstream flame front thickness (filled) and autoignition spot longitudinal half-size (empty) as a function of  $L_{\text{MIN}}$  for n-heptane with:  $T_{\text{air}} = 1100\text{--}1120\text{K}$ ,  $U_{\text{air}} = 14\text{m/s}$ ,  $Y_{\text{fuel}} = 0.95$ ,  $u_{\text{inj}} = 1.0$  (circles), and,  $T_{\text{air}} = 1100\text{--}1140\text{K}$ ,  $U_{\text{air}} = 18\text{m/s}$ ,  $Y_{\text{fuel}} = 0.95$ , and,  $u_{\text{inj}} = 1.0\text{--}1.2$  (squares).**

The mean front thickness is little affected by the conditions and  $L_{\text{MIN}}$ , remaining in the range 3.0–3.5mm. However, the spot size  $\langle Z_{\text{spot}} \rangle$  increases slightly with  $L_{\text{MIN}}$  for the same  $U_{\text{air}}$  and with  $U_{\text{air}}$  for the same  $L_{\text{MIN}}$ , going from 5.5 to 7.5mm. In fact, it increases almost linearly with increasing  $L_{\text{MIN}}$ , perhaps suggesting a link with the mean plume width (perhaps of the lean flammability limit composition) at the axial length where autoignition occurs that also increases linearly with  $z$ . At long  $L_{\text{MIN}}$ , we expect  $\langle Z_{\text{spot}} \rangle$  to be largest, because the plume is widest and adequate mixing has introduced finite flammable mixture across a greater extent of the tube. At the limit of autoignition at  $L_{\text{MIN}} \approx 85\text{mm}$ , indeed,  $\langle Z_{\text{spot}} \rangle$  is at its largest (about 7.5mm). The mean composition at the longest  $L_{\text{MIN}}$  will be nearest to  $\phi_{\text{PM}}$ . The ‘premixed’ equivalence ratio  $\phi_{\text{PM}}$ , is defined as the equivalence ratio after complete mixing between the air and nitrogen-diluted n-heptane. For these experiments  $\phi_{\text{PM}} = 0.4\text{--}0.5$ , near the lean flammability limit,  $\phi_{\text{LFL}}$ , of 0.53 [17]. In addition, from 0-D Conditional Moment Closure (CMC) [2],  $\xi_{\text{MR}} = 0.09\text{--}0.14$ , corresponding to  $\phi_{\text{MR}} = 1.4\text{--}2.3$ .

Similar results were obtained for acetylene, with  $\langle Z_{\text{spot}} \rangle$  between 8–10mm. Hydrogen spots and upstream reaction zones were found to be smaller and thinner respectively, agreeing with [2] where it was noted that the two-dimensional pdfs of autoignition (contaminated by post-ignition combustion of the spots) were much thinner in their radial extent for this fuel. The mean flame front thickness was found to be 1–3mm, while  $\langle Z_{\text{spot}} \rangle$  was between 2–5mm. These values should be compared with equivalent results for the hydrocarbon fuels. Clearly, the hydrogen reaction zones extinguish much closer to the original explosions than what was measured for the hydrocarbons. Possibly, this can be explained in terms of  $\xi_{\text{MR}}$  for hydrogen, which, at 0.007–0.035 (or an equivalence ratio of 0.2–0.3), was

leaner by an order of magnitude than that of n-heptane and  $\phi_{\text{PM}}$  for hydrogen, which in these experiments was about 0.015–0.021. In addition, the lean flammability limit for hydrogen is  $\phi_{\text{LFL}} = 0.10$  [17]. Consequently, the initial appearance of the flame will be situated farther away from the stoichiometric contour and the bulk of the mixture into which the flame will be propagating will be well beyond the flammability limits that would allow the flames to propagate. Recall that for n-heptane unlike hydrogen,  $\phi_{\text{PM}} (= 0.4\text{--}0.5)$  was near  $\phi_{\text{LFL}} (= 0.53)$ .

### Flame Front and Autoignition Spot Advection Velocities

Figure 8 shows pdfs for the absolute (relative to the injector and tube) velocities obtained from the data of Fig. 6, namely the propagation velocities of the upstream flame fronts and those of the (geometrical center of the) spots.

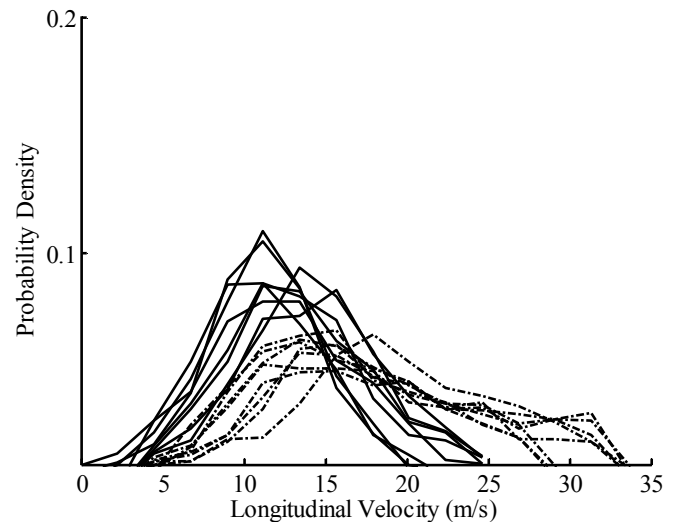


**Figure 8. Pdfs of upstream flame front (solid) and autoignition spot center advection (dash-dot) velocity for n-heptane. Conditions as in Fig. 6.**

It is important to note that the velocities are both positive. In other words, all reaction zones (including the upstream ones) move downstream and away from the injector. This is important because it suggests that within any instantaneous image, limited information of the downstream extent of the spot ( $z_{\text{dn}}$ ) might be lost due to the finite exposure time, but not so for the upstream extent ( $z_{\text{up}}$ ). Based on the pdfs in Fig. 8, we calculated the mean absolute longitudinal velocities that are plotted against  $L_{\text{MIN}}$  in Fig. 9(a). The mean spot velocity  $\langle U_{\text{spot}} \rangle$  (empty symbols), both for the  $U_{\text{air}} = 14\text{m/s}$  (circles) and 18m/s (squares) data, was found to be within  $0.90\text{--}1.05U_{\text{air}}$ , leading one to remark that the spots must be advected by the mean flow. In addition, this was checked for the case of the point of peak intensity as well and it was found that  $\langle U_{\text{pk}} \rangle / U_{\text{air}} = 0.95\text{--}1.10$ . As an aside, the longitudinal velocities of the fronts downstream of the geometric center were greater than the corresponding upstream ones, or  $U_{\text{up}} < U_{\text{spot}} < U_{\text{dn}}$ . In fact, it was found that the longitudinal velocity of the upstream flame fronts was found to be about 70–75% of that of the point of peak intensity and about 60–80% of that of the downstream flame fronts. Moreover, the velocity of the point of peak intensity  $\langle U_{\text{pk}} \rangle$  was about 10% higher than that of the geometric center of the spot,  $\langle U_{\text{spot}} \rangle$ . The above findings imply

that,  $U_{up} < U_{pk} \approx U_{spot} \approx U_{air} < U_{dn}$ , meaning that  $S_T (= \langle U_{up} \rangle - U_{air})$  is negative. Recognizing that the general trend is for  $|S_T|$  to decrease with  $L_{MIN}$  (explained below) the fact that  $U_{up} < U_{dn}$  implies that  $\langle U_{dn} \rangle$  is affected by density (product gas expansion) effects. For this reason, we use the velocity of the point of peak intensity  $\langle U_{spot} \rangle = d\langle z_{pk} \rangle / dt$  as the best spot 'advection' velocity and consider only the propagation of the upstream flame fronts for the estimation of  $S_T$ ,  $S_T = U_{up} - U_{air}$ .

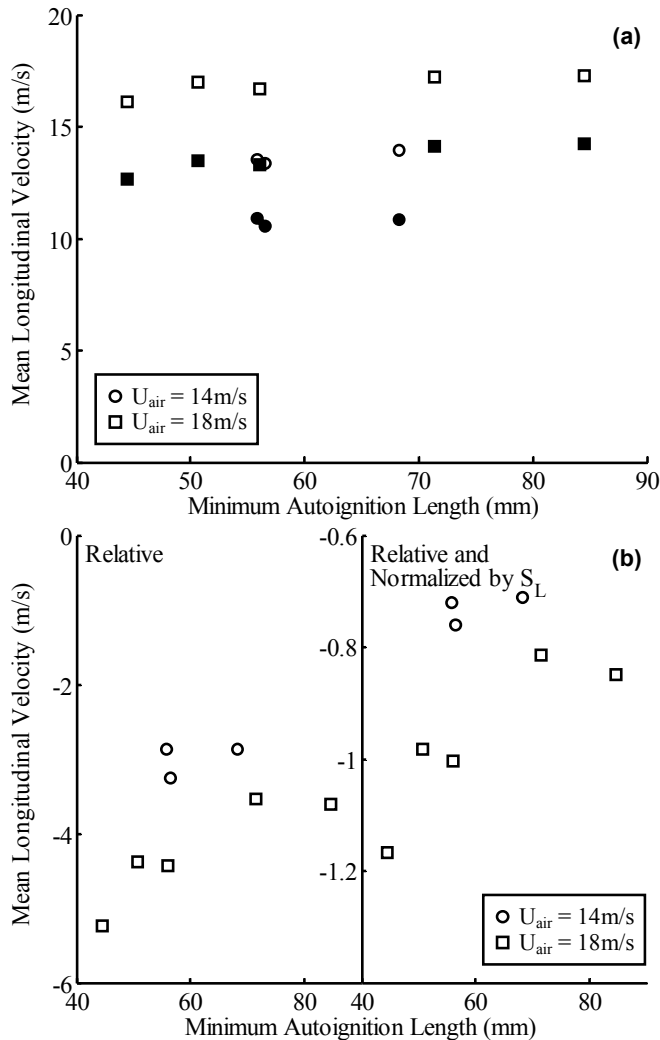


**Figure 9. Mean velocities as a function of  $L_{MIN}$  for n-heptane with conditions as in Fig. 6. (a) Absolute longitudinal upstream flame front (solid) and autoignition spot advection (empty) velocities. (b) Upstream longitudinal flame front velocity.**

Figure 9(b) contains the same data as in (a), but relative to the oncoming flow, with  $S_T$  (left) and  $S_T$  normalized by the laminar flame speed for those conditions (right). The upstream fronts of the spots move against the flow at a speed of the order of  $S_L$ , even though their resultant motion is still downstream. We predict then that when  $S_L > U_{air}$ , Flashback will ensue. Yet, the relative speed of the upstream fronts decrease with increasing  $L_{MIN}$ , more than what can be accounted for by the change in  $S_L$  in the domain. This is an interesting finding and can be explained in terms of the decrease in  $\chi$  at longer  $z$  (and

hence  $L_{MIN}$ ), augmented by the decrease in  $\text{pdf}(\xi)$  at the compositions close to  $\xi_{ST}$  associated with higher flame speeds.

In the radial direction, Fig. 10,  $\langle V_{spot} \rangle$  was between 2–3 m/s, about  $0.6\text{--}0.7\langle U_{spot} \rangle$  or  $0.5\text{--}0.6S_L$ , also decreasing with increasing  $L_{MIN}$ . This finding is consistent with the previously stated result of spots slightly elongated in the axial direction by up to 20%. Since the propagation in the radial direction is, on average, unaffected by the bulk motion of the flow, the fact that the trend of  $\langle V_{spot} \rangle$  in Fig. 10 and the magnitude of  $\langle V_{spot} \rangle / S_L$  closely resemble the longitudinal data (trends and magnitude of  $S_T$ ) gives credence to our previous estimates for  $S_T$ .

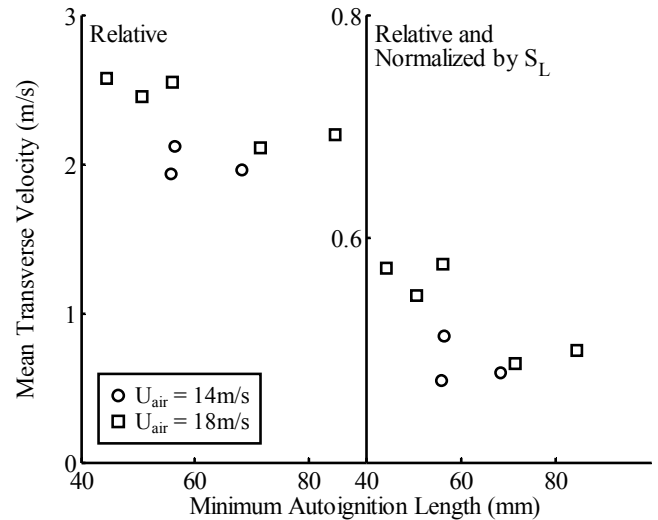


**Figure 10. Mean transverse velocity of left and right flame fronts for n-heptane with conditions as in Fig. 6.**

Having considered the case of n-heptane so far, we turn our attention to acetylene and hydrogen. Figure 11 shows longitudinal upstream flame front velocities, both absolute, relative (left) and relative to  $U_{air}$  and normalized by the laminar flame speed (right). The absolute flame velocities varied from 15 to 26 m/s for acetylene and from 6.5 to 8.5 m/s for hydrogen. Yet, we note that the relative propagation of these flame fronts is once again near the laminar flame speed, but also that the  $S_T$  decreases as autoignition/propagation occurs at longer  $L_{MIN}$ .

To summarize briefly, we have used three different fuels (and hence  $\xi_{ST}$ ,  $\xi_{MR}$ ,  $\phi_{PM}$ ), a wide range of nitrogen-dilutions, temperatures and velocities, obtaining flame velocity data at ultimately different autoignition lengths in a fixed geometry. For all tested fuels, a consistent result emerges concerning the upstream flame front velocity,  $S_T$ . Firstly, its direction is positive, but relative to  $U_{air}$  this becomes negative. In other words, the upstream flame fronts in the autoignition spots travel downstream in an absolute sense, but upstream relative to the oncoming flow. Secondly, the magnitude of the upstream flame front velocity or flame speed,  $|S_T|$ , remains of the order of the laminar flame speed,  $S_L$ , in agreement with [8], while there is a slight trend for  $|S_T|$  to decrease with increasing  $L_{MIN}$ , dropping below  $S_L$  at long  $L_{MIN}$ , and, to increase even at the same  $L_{MIN}$  if  $U_{air}$  is higher. Despite the fact that the flow is turbulent and the mixture is not frozen, the flamelet propagation speed seems to be of the order of the laminar burning velocity. This may be because, following autoignition at  $\xi_{MR}$ , the flamelet propagates in mixtures with composition far from stoichiometry.

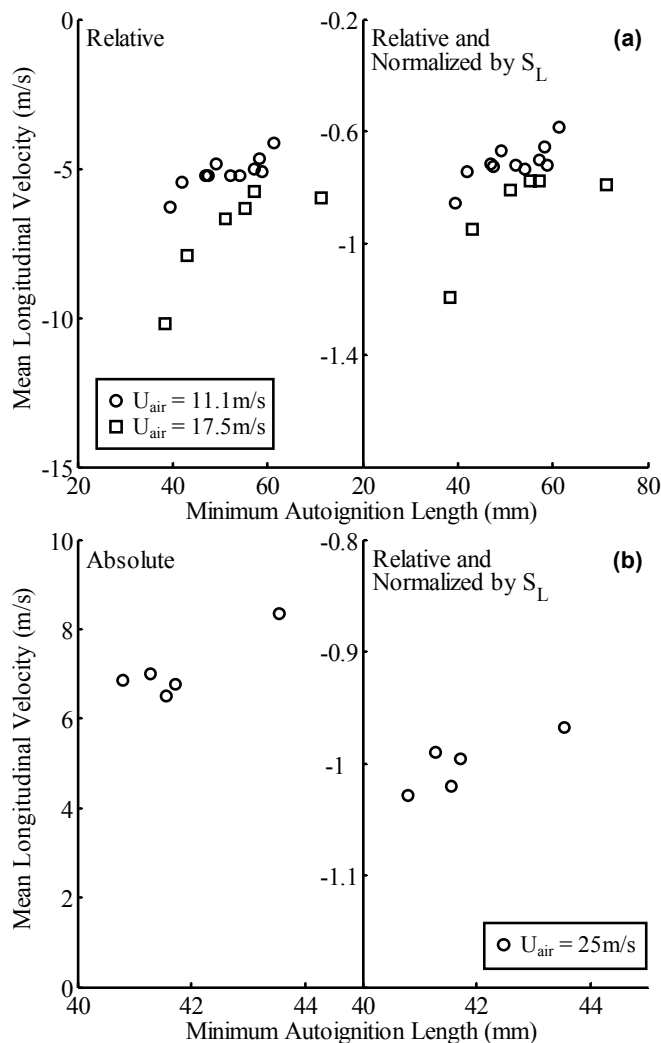


**Figure 11. Mean longitudinal upstream flame front velocities as a function of  $L_{MIN}$ . (a) Acetylene with:  $U_{air} = 11.1$  m/s,  $T_{air} = 806-824$  K,  $Y_{fuel} = 0.6$ ,  $U_{inj} = 1.0$  (circles), and,  $U_{air} = 17.5$  m/s,  $T_{air} = 850-879$  K,  $Y_{fuel} = 0.6$ ,  $U_{inj} = 1.0$  (squares). (b) Hydrogen with:  $T_{air} = 950$  K,  $U_{air} = 25$  m/s,  $Y_{fuel} = 0.2-1.0$  and  $U_{inj} = 0.9-1.0$ .**

### Evolution of the Propagation Velocities

It is common for the extinction process to appear as one in which the overall size of the spot diminishes. It has been previously stated that the propagation velocities were a function of the time from explosive autoignition (see Fig. 1) and that the reported value of velocity of each flame front was defined as the average distance traveled from the moment of explosive autoignition to the time the chemiluminescence intensity reached 5% of its maximum value. This was chosen to correspond approximately to the condition for the growth of a spot, i.e.  $dZ_{spot}/dt > 0$  or  $dR_{spot}/dt > 0$ , as demonstrated in Fig. 12.

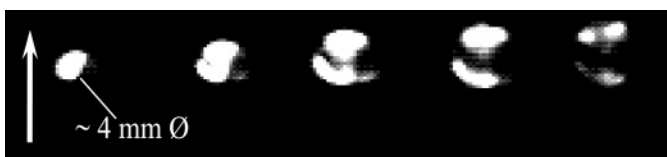


**Figure 12. Evolution of spot flame fronts at 13.5 kHz. Flow direction shown and scale given. Reproduced from [1].**

In this section, we quantify the temporal evolution of the propagation velocities with acetylene data. Figure 13(a) shows the mean time taken for the intensity of the spots to decay to three different fractions of their maximum value.

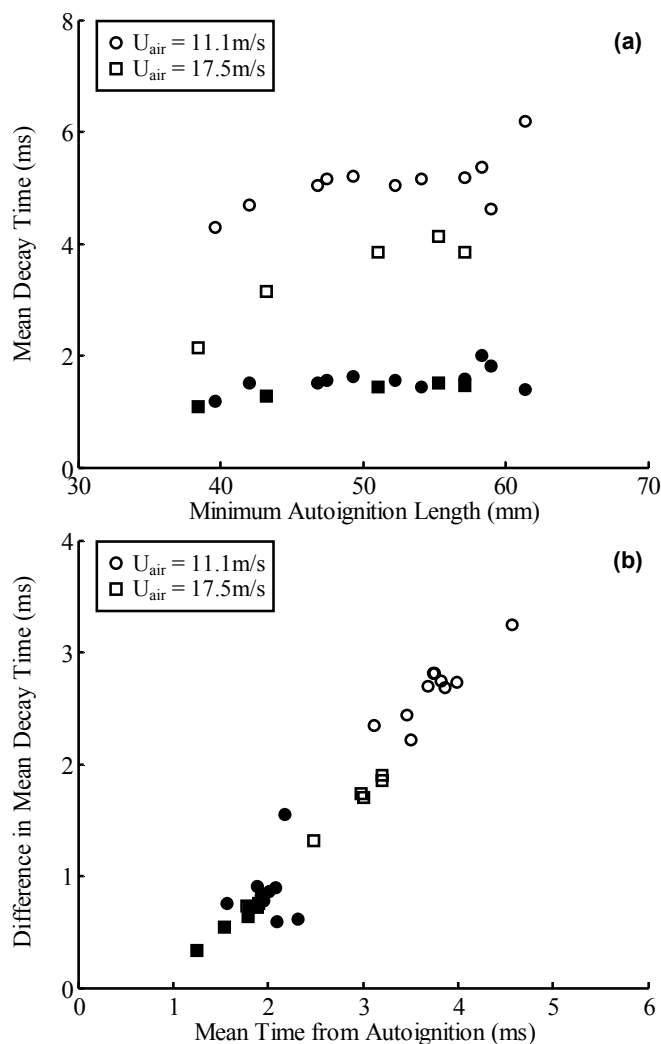


**Figure 13. (a) Mean acetylene decay time from instant of autoignition to 10% (solid) and 1% (empty) decay thresholds as a function of  $L_{MIN}$ . Conditions as in Fig. 11(a). (b) Difference in mean decay time as a function of the time from autoignition, from 10 to 5% (solid) and 5 to 1% (empty) decay thresholds. Calculated based on data in (a).**

The maximum value is attained about 0.5 ms after the explosive emergence of autoignition. The mean decay time increases with increasing  $L_{MIN}$  for all thresholds, reflecting the fact that as autoignition occurs farther downstream the propagation velocity decreases, consistent with the direct velocity results. Note that the time to decay to 10% of the maximum, unlike the decay to 1%, is only dependent on  $L_{MIN}$  and not affected by  $U_{air}$  for the same  $L_{MIN}$ . This might suggest that the former is mostly dependent on the flow geometry, in that the spot intensity will reach this level when it has reached a certain (such as  $\phi_{PM}$  or  $\phi_{LFL}$ ) extent of the plume. We may also speculate that the latter depends additionally, perhaps, on the local micro-mixing (including the pdf( $\xi$ )) and the conditional  $\chi(\xi)$  at the regions where the propagation is taking place.

Going a step further, Figure 13(b) shows a clear positive correlation between the rate of decay of the spot intensity and the mean time from autoignition at which the rate is evaluated. This would have been expected, for example, by considering the decreasing modulus of the gradient in the profile in Fig. 1. Physically, this represents the extinction process of the spots as the flame fronts propagate from  $\xi_{MR}$  towards leaner and richer mixtures that tend to decrease the flame speed. In addition, the data points from the higher velocity case (squares) have a higher rate of decay (lower difference in decay time), perhaps corresponding to the known higher  $\chi$  at those locations [2, 12].

## CONCLUSIONS

The autoignition of axisymmetric plumes of pure or nitrogen-diluted hydrogen, acetylene and n-heptane, injected continuously into turbulent, hot co-flows of air has been visualized with a high-speed intensified camera. Localized autoignition and post-ignition flame phenomena have been observed, including a statistically steady Random Spots and a Flashback behavior. The boundary between these regimes of operation has been explored. It was found that the onset of Flashback was shifted to higher air temperatures with higher velocities and smaller injector diameters.

In the Random Spots regime, as the air temperature increased and/or air velocity decreased, the autoignition regions moved (upstream) towards the injector. After a localized explosive autoignition event, flames propagated in all directions into the unburnt mixture and eventually (after a few ms) extinguished, giving rise to autoignition 'spots' of mean radius 2–5mm for hydrogen and 6–10mm for the hydrocarbons. The average flame propagation velocities varied from 0.5–1.2 $S_L$ , where  $S_L$  is the laminar burning speed of the stoichiometric mixture. This was not expected, especially given the turbulent nature of the flow and the chemically evolved state at the locations of autoignition, but is consistent with previous DNS results [8] and can be attributed to the fact that most of this propagation occurs at mixtures very different from stoichiometric. The propagation velocities were found to increase as the autoigniting regions shifted upstream, perhaps due to the mixture composition and/or the increase in the scalar dissipation rate in those regions. Further experiments in different flow geometries such as with a smaller injector or a modified turbulence grid can help to clarify some of these results. In future, it is also important to verify these findings with detailed planar optical measurements.

## ACKNOWLEDGMENTS

We thank Dr. Ivor Day for lending us his Dantec Constant Temperature Anemometer unit, Mr. Ed Richardson for undertaking the premixed laminar flame speed calculations and Mr. Giorgio De Paola for the 0-D CMC calculations. Figure 1 has been reprinted from Markides [2]. Figure 12 has been reprinted from Markides and Mastorakos [1] with permission from Elsevier. This work has been funded by EPSRC.

## REFERENCES

[1] Markides, C. N., and Mastorakos, E., 2005, "An Experimental Study of Hydrogen Autoignition in a Turbulent Co-Flow of Heated Air," *Proceedings of the Combustion Institute*, **30**, pp. 883–891.

- [2] Markides, C. N., 2005, "Autoignition in Turbulent Flows," Ph.D. thesis, University of Cambridge, U.K.
- [3] Markides, C. N., De Paola, G., and Mastorakos, E., 2005, "Measurements and Simulations of Mixing and Autoignition of an N-Heptane Plume in a Turbulent Flow of Heated Air," *Proceedings, Mediterranean Combustion Symposium*.
- [4] Ballal, D. R., and Lefebvre, A. H., 1979, "Ignition and Flame Quenching of Flowing Heterogeneous Fuel—Air Mixtures," *Combustion and Flame*, **35**, pp.155–168.
- [5] Kaminski, C. F., Hult, J., Alden, M., Lindenmaier, S., Dreizler, A., Mass, U, and Baum, M., 2000, "Spark Ignition of Turbulent Methane/Air Mixtures Revealed by Time-resolved Planar Laser-Induced Fluorescence and Direct Numerical Simulations," *Proceedings of the Combustion Institute*, **28**, pp. 399–405.
- [6] Ko, Y. S., and Chung, S. H., 1999, "Propagation of Unsteady Tribachial Flames in Laminar Non-premixed Jets," *Combustion and Flame*, **118**, pp. 151–163.
- [7] Ahmed, S. F., and Mastorakos, E., 2005, "Spark Ignition of Lifted Turbulent Flames," *Combustion and Flame*, to appear.
- [8] Mastorakos, E., Baritaud, T. B., and Poinot, T. J., 1997, "Numerical Simulations of Autoignition in Turbulent Mixing Flows," *Combustion and Flame*, **109**, pp. 198–223.
- [9] Edwards, C. F., Siebers, D. L., and Hoskin, D. H., 1992, "A Study of the Autoignition Process of a Diesel Spray via High Speed Visualization," *SAE Technical Paper*, **920108**, pp. 1–18.
- [10] Arnold, A., Dinkelacker, F., Heitzmann, T., Monkhouse, P., Schafer, M., Sick, V., Wolfrum, J., Hentschel, W., and Schindler, K. -P., 1992, "Di Diesel Engine Combustion Visualized by Combined Laser Techniques," *Proceedings of the Combustion Institute*, **24**, pp. 1605–1612.
- [11] Murase, E., Hanada, K., Miyaura, T., and Ikeda, J., 2005, "Photographic Observation and Emission Spectral Analysis of HCCI Combustion," *Combustion Science and Technology*, **177**, pp. 1699–1723.
- [12] Markides, C. N., and Mastorakos, E., 2006, "Measurements of Scalar Dissipation in a Turbulent Plume with Planar Laser-Induced Fluorescence of Acetone," *Chemical Engineering Science*, to appear.
- [13] Rotexo GmbH & Co. KG, 2005, *COSILAB: The Combustion Simulation Laboratory*, www.SoftPredict.com, **Version 1.2.3**, Haan, Germany.
- [14] Connaire, M. O., Curran, H. J., Simmie, J. M., Pitz, W. J., and Westbrook, C. K., 2004, "A Comprehensive Modeling Study of Hydrogen Oxidation," *International Journal of Chemical Kinetics*, **36**, pp. 603–622.
- [15] Held, T. J., Marchese, A. J., and Dryer, F. L., 1997, "A Semi-Empirical Reaction Mechanism for N-Heptane Oxidation and Pyrolysis," *Combustion Science and Technology*, **123**, pp. 107–146.
- [16] Laskin, A., and Wang, H., 1999, "On Initiation Reactions of Acetylene Oxidation in Shock Tubes. A Quantum Mechanical and Kinetic Modeling Study," *Chemical Physics Letters*, **303**, pp. 43–49.
- [17] Glassman, I., 1996, *Combustion*, Academic Press, San Diego, pp. 163 & 581–587.